Treatment of Biotreated Coking Wastewater by a Heterogeneous Electro-Fenton Process Using a Novel Fe/Activated Carbon/Ni Composite Cathode

Yanqiu Wang[1,2], Xinyu Zhou[1], Nan Jiang[1,3], Guangcai Meng[1], Jinfeng Bai[1,2,], Yanli LV[1,2]*

[1] School of Chemical Engineering, University of Science and Technology Liaoning, Anshan 114051, P.R. China
[2] Engineering Research Center of Advanced Coal & Coking Technology and Efficient Utilization of Coal Resources, the Education Department of Liaoning Province, Anshan 114051, P.R. China
[3] Grinm Semiconductor Materials Co., Ltd., Beijing 100088, P.R. China
[*]E-mail: baijf863@126.com

A novel composite electrode was successfully developed that consisted of an activated carbon-supported iron salt and foamed nickel as the electrode material. Heterogeneous electro-Fenton (HEF) technology was applied to treat the biotreated coking wastewater (BTCW) with the electrode performing as the cathode. A response surface methodology combined with a single factor discussion was used to investigate individual parameters and the interaction of the three main parameters, namely, the applied voltage, plate spacing and initial pH; the removal rate of the COD from the BTCW was selected as the response index. The results demonstrated that the plate spacing was the most influential parameter under the selected conditions. The optimized conditions, which were based on a Box-Behnken design (BBD), were as follows: applied voltage: 10 V, plate spacing: 1 cm, and initial pH: 3.42. Under these conditions, the COD removal efficiency could reach almost 100% after reacting for 3 h. A spectroscopic analysis showed that the process could effectively remove aromatic protein analogs, microbial byproduct analogs, lactones and amide compounds in the coking wastewater. In addition, repetitive experiments indicated that the prepared electrode demonstrated good reusability. Therefore, the application of the novel composite electrode in the HEF process shows promising prospects for degrading organic contaminates in wastewater.

1. INTRODUCTION

Coking wastewater is generally produced by the steel industry in the process of coal coking and gas purification, and in the refining and recovery of chemical products. The resulting water quality is

complex, with an abundance of species from organic sources and inorganic matter [1]. Most of the inorganic pollutants are ammonium salts, while the organic pollutants are mainly phenolic compounds with a high toxicity [2,3]. Thus, coking wastewater is a typical industrial wastewater with a high concentration of refractory organic matter. The process for treating coking wastewater generally includes a pretreatment, biological treatment, and advanced treatment [4]. The pretreatment is to assist the biological treatment, and a physicochemical method is an often used method, including solid precipitation, degreasing, cyanide removal, phenol degradation, etc. The biological treatment plays the most important role in the removal of both inorganic ammonia salts and organic pollutants. Currently, common processing methods include anoxic oxic (AO) or anaerobic-anoxic-oxic (A/A/O) and sequencing batch reactors (SBRs) [5–7]. The Biological treatment is environmentally friendly and cost-effective in addressing most organic pollutants [8]. However, the treatment of the high contents of nitrogen-containing heterocylic and polycyclic aromatic hydrocarbon compounds found in coking wastewater is limited, which may be attributed to the inhibitory effects of toxic compounds during the biodegradation process[3]. The above result leads to the BTCW being unable to reach the current wastewater discharge standard, and a certain amount of these substances may affect the environment and human health [4,9]. The advanced treatment is to improve the intensity of the treatment for difficult biodegradable organic matter to achieve effluent discharge standards, which is simply an urgent problem that needs to be solved.

With the continuous development and improvement of science and technology, advanced oxidation technology has been gradually applied to water treatment processes [10,11]. The main method is to generate hydroxyl radicals (•OH) with strong oxidizing ability; the oxidation reaction continues until a full mineralization to CO_2, water and inorganic ions is achieved, especially for organic pollutants that are hard to biodegrade [3,12–14]. Among the advanced oxidation technologies, traditional Fenton technology lays the foundation that employs mild oxidation reaction conditions, obvious treatment effects, convenient operation and simple equipment [11]. The performed reaction process is based on the electron transfer between hydrogen peroxide (H_2O_2) and a homogeneous metal catalyst (Fe^{2+}). The Fenton reaction mechanism can be expressed by the following equations:

$$Fe^{2+}+H_2O_2 \rightarrow Fe^{3+}+\cdot OH+OH^- \quad (1)$$
$$Fe^{3+}+H_2O_2 \rightarrow Fe^{2+}+\cdot HO_2+H^+ \quad (2)$$
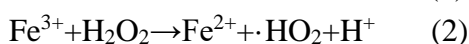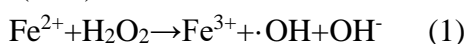
However, during the reaction process, the different rate constants of Equation (1) and Equation (2) cause the consumption rate of Fe^{2+} to be inconsistent with the regeneration rate, which results in the formation of a large amount of iron sludge caused by the catalytic cycle; additionally, there are also risks in the transportation, storage, and handling of H_2O_2 [3,15]. Compared with conventional Fenton technology, electro-Fenton (EF) technology reduces the dosing of H_2O_2, and instead, produces H_2O_2 by the reduction of oxygen or air at the cathode by an electrochemical reaction [16]. Since Fe^{3+} produced by the Fenton reaction can be reduced to Fe^{2+} at the cathode, only a small amount of Fe^{2+} is added as a source of Fenton's reagent [12]. Even when the initial reaction rate of H_2O_2 at the cathode is not high, the Fenton reaction can react continuously. The recycling of Fe^{2+} is accelerated by electrolysis in which the amount of catalyst is increased to a certain extent, and the production of ferrous sludge is greatly decreased; thus, resources are saved and the environmental impact is reduced. A homogeneous electro-Fenton system requires the reaction to proceed under acidic conditions, can

make the utilization of iron salts and hydrogen peroxide difficult [17]. Some improved EF technology is available to reduce the encountered difficulties [18]. Among them, the development of a heterogeneous electro-Fenton (HEF) system has received great attention. Using a solid catalyst as an electrode material to prepare a composite electrode is one of the most promising modes in an HEF system [19]. At present, commonly used electrode carrier materials are carbon materials such as activated carbon and graphite felt because micro/mesoporous materials have strong adsorption performance, which is favorable for multiphase reactions and iron loading [15,19]. In this study, a novel foamed nickel composite electrode with iron salt (divalent iron ion) supported on activated carbon (Fe-AC-Ni composite electrode) was prepared by impregnation and calcination. Activated carbon was used as the catalyst carrier due to its chemical stability, while its strong adsorption performance and large specific surface area were desirable during the course of oxidation. The foamed nickel, which exhibits strong electrical conductivity and outstanding physical properties and also contains a good three-dimensional structure and transparent holes, was selected as the electrode surface material and could improve the utilization of electric current [20]. Furthermore, it has been reported that the amount of H_2O_2 produced by cathodes with nickel foam is greater than that with other materials [19].

The purpose of this study is to verify that the Fe-AC-Ni composite electrode combined with a dimensionally stable anode (DSA) is efficient in the disposal of BTCW, which is taken as an example to indicate that the facility can effectively degrade organic-contaminated wastewater. The experiment was designed using BBD, while the experimental data were analyzed by Design Expert 8.0 software [21]. Then, a quadratic regression model of the applied voltage, plate spacing and initial pH to the COD removal rate of the BTCW was established. We obtained the optimum process conditions and analyzed the significant factors affecting the COD removal rate by response surface methodology (RSM). Ultraviolet-visible spectroscopy (UV-Vis), three-dimensional (3D) fluorescence spectroscopy, Fourier transform infrared (FTIR) spectroscopy, and gas chromatography-mass spectrometry (GC-MS) were used to analyze the types and concentrations of the organic matter in the BTCW before and after the reaction to confirm the processing effect.

2. EXPERIMENTAL

2.1. Characteristics of the target wastewater

The BTCW used in this study was from a coking wastewater treatment station of a steel plant located in Liaoning, China, which had been subjected to steaming ammonia, gravity, air flotation and oil removal, and A/A/O biochemical treatments. The sample was obtained from the supernatant of the secondary sedimentation tank. The main characteristics of the BTCW are shown in Table 1.

Table 1. Characteristics of the BTCW

Parameter	COD ($mg·L^{-1}$)	NH_3-N ($mg·L^{-1}$)	pH	Conductivity ($mS·cm^{-1}$)	Chromaticity (times)
Value	250.52	0	8.45	4.16	50

2.2. Materials

In this experiment, the solutions were prepared with deionized water. Ferrous sulfate and other chemicals were analytical reagents supplied by Sinopharm Chemical Reagent Co., Ltd. Ti-base and RuO_2-IrO_2-coating mesh DSA anodes were provided by Titanium Nickel Gold Port Equipment Manufacturing Co., Ltd. The activated carbon was coconut shell activated carbon obtained from Anshan City Activated Carbon Factory. Polytetrafluoroethylene (PTFE) and acetylene black were purchased from Lizhiyuan Battery. The acetylene black was battery grade.

2.3. Preparation of the Fe-AC-Ni composite cathode

The proper amount of activated carbon material was washed with 100 mL NaOH solution (0.02 M) and subsequently washed with distilled water until neutral. Then, the solution was pickled in 100 mL of H_2SO_4 solution (0.02 M) and washed with distilled water to neutral. The activated carbon material was dried in an electric drying oven at a temperature of 110 °C and then cooled to room temperature. A 1% Fe^{2+} iron salt solution was supported on the activated carbon material via an impregnation method [22]. The sample was placed in a tube furnace, calcined at 300 °C under high purity nitrogen, and then cooled to room temperature; the catalyst was prepared well. Catalyst, binder (PTFE), and conductive agent (acetylene black) were mixed according to a mass ratio of 16:5:1 and was then placed in an ultrasonic reactor container and mixed as evenly as possible with an appropriate amount of absolute ethanol. After ultrasonication, the container was placed on a heater and stirred with the temperature controlled at 78 °C (below the boiling point of alcohol). The absolute ethanol was gradually evaporated from the mixed material until the mixed material gradually formed a paste. A sheet electrode was made by a rolling method. Two pieces of appropriately sized foamed nickel were cut into an electrode skeleton (70 mm×100 mm). The sheet electrode was put into the two pieces of foamed nickel and tightly combined under a pressure of 10 MPa by a YP-2-type pressing machine.

2.4. Experimental procedure

The experiment was carried out at room temperature. The device consisted of an SG1731SC3A DC stabilized current source, reaction tank, electrode and aeration pump. The reaction tank was a plexiglass tank with a volume of 800 mL. DSA was used as the anode (40 mm×60 mm), while the Fe-AC-Ni composite electrode was used as the cathode (40 mm×60 mm). The pH of the BTCW was adjusted to a desired level with solutions of NaOH and H_2SO_4 (0.01 M). Aeration was carried out for 30 min before the start of electrolysis. The applied voltage in the reaction device was controlled through a DC-stabilized current source. The aeration pump supplied air to the device and at the same time provided sufficient agitation through aeration.

2.5. Experimental design

RSM is a very effective statistical method for solving multiple variables. It is a comprehensive application combining experimental design, data statistics and parameter optimization. It is often used to analyze a modeling and analysis problem whose response value is affected by many factors, with the goal of optimizing the response value[23]. RSM requires fewer experiments than other methods and demonstrates high experimental precision, a short experimental period, and a wide application range, which plays an important role in solving practical application problems[24].

In this work, a BBD experiment was used to optimize the cathode EF oxidation process. The BBD was designed as a spherical rotation model that consisted of a central point and the middle points of cube edges circumscribed on a sphere. Three important factors, namely, the applied voltage (X_1), plate spacing (X_2) and initial pH (X_3), were investigated to evaluate the removal efficiency of COD from the BTCW. As shown in Table 2, the range and level of the three variables were determined, while each independent variable was coded at three levels between 1 (high), 0 (middle) and -1 (low) [25]. A total of 17 sets of comparative experiments were performed in this study based on the interaction of applied voltage, plate spacing and initial pH, including twelve factorial tests and five duplicates at the center point (used to determine the experimental error). The experimental data were analyzed by using Design-Expert 8.0 software, and an empirical variable second-order polynomial model was used to associate the response variable Y with the independent variable. The generalized model is as follows:

$$Y = b_0 + \sum_{j=1}^{k} b_i X_i + \sum_{j=1}^{k} b_{ii} X_j^2 + \sum_{i=1}^{k} \sum_{j>1}^{k} b_{ij} X_i X_j + \varepsilon$$

where Y is the response variable for the COD removal efficiency; X_i is the input variable that affects the response; X_j^2 is the square effect; $X_i X_j$ is the interaction effect; b_0 is the intercept coefficient; b_i is the regression coefficient of the linear effect; b_{ii} is the regression coefficient of the square effect, additionally, the interaction effect of b_{ij} and the regression coefficient of X_i are the experimental levels of the variables; ε is the error; and k is the number of independent parameters ($k=3$ in this study).

Table 2. Coded and actual values of the independent variables used in the Box-Behnken design

Independent variables	Factors	Coded levels		
		-1	0	1
Applied voltage (V)	X_1	8	9	10
Plate spacing (cm)	X_2	1	2	3
Initial pH	X_3	2	3	4

2.6. Analytical methods

The COD was determined by the potassium dichromate method (China national standard: GB11914-89). Chroma was measured using a multiple dilution method (China national standard: GB/T11903-1989). Scanning electron microscopy was performed to observe the surface morphology

of the activated carbon and Fe-AC-Ni composite electrode. The BTCW before and after the HEF treatment reaction with the Fe-AC-Ni composite electrode was analyzed by using GC-MS, UV-Vis scanning, FTIR spectroscopy and three-dimensional fluorescence excitation-emission matrix (3D-EEM) spectroscopy.

The instrument model used in the GC-MS analysis was 7890A/5975C (Agilent Corporation, American), and was equipped with an HP-5MS column with an inner diameter of 0.25 mm, a length of 30 m and a film thickness of 0.25 μm. Before the sample was placed, it was first extracted with CH_2Cl_2 into three primary phases, namely, acidic, neutral and alkaline, and then mixed. An appropriate amount of Na_2SO_4 was added to absorb water and break the emulsion. Finally, the extract phase was placed in a rotary evaporator for concentration and purged with high-purity nitrogen. While waiting for the analysis, the oven temperature was kept at 60°C for 2 min, increased by 5°C/min to 110°C for 10 min, and then increased by 25°C/min to 280°C for 15 min. The electron energy was 70 eV.

At a scanning speed of 266 nm/min, the water sample was diluted 50 times, and ultrapure water was used as a reference object for UV-Vis scanning. The wavelength range was 190-800 nm, and the width of the slit was 2 nm.

For FTIR spectroscopy, after the water sample was dried, the residual solid was collected and stored in a dry box. Then, dried KBr was mixed with an appropriate amount of solid sample, and they were placed in an agate mortar and uniformly ground for approximately 10 min. The powder was placed in a YP-2 tableting machine and compressed at 15 MPa. A KBr sheet was used as a blank control sample, and the substrate was removed by scanning with a Nicolet iS10 infrared spectrometer (Nichols Corporation, USA).

Fluorescence scanning was performed with an LS55 fluorescence scanner (PerkinElmer, Co, USA). First, the water sample was diluted to control the COD of the water sample at 3-6 mg·L^{-1}, while the scanning speed was set to 1200 nm/min. An automatic mode was used for the response time. The excitation wavelength was 200-450 nm, while the emission wavelength was 280-550 nm; the scanning steps were 5 nm and 2 nm. The excitation and emission slit width was 5 nm.
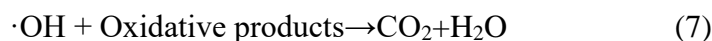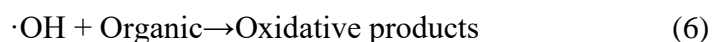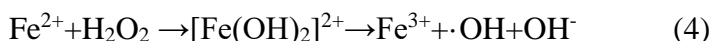
3. RESULTS AND DISCUSSION

3.1. Influencing factors of the BTEW treatment

3.1.1 Effect of applied voltage

In the HEF system for the treatment of the BTCW, the applied voltage is the driving force of the electrochemical reaction. The effects of the applied voltage on the COD removal rate were investigated by varying the voltage from 4 V to 10 V. As shown in Figure 1, when the applied voltage is 10 V, the treatment effect of the cathode EF oxidation system on the BTCW is the best, and the removal rate reaches 84.79%. As the applied voltage increases, the electrochemical reduction of oxygen is accelerated. It also increases the rate of H_2O_2 and ·OH formation, which accelerates the

Fenton reaction rate and increases the rate of organic matter degradation. The degradation can be expressed as shown in the following equations [26]:

$$O_2 + 2H^+ + 2e^- \rightarrow H_2O_2 \tag{3}$$

$$Fe^{2+} + H_2O_2 \rightarrow [Fe(OH)_2]^{2+} \rightarrow Fe^{3+} + \cdot OH + OH^- \tag{4}$$

$$Fe^{3+} + e^- \rightarrow Fe^{2+} \tag{5}$$

$$\cdot OH + Organic \rightarrow Oxidative\ products \tag{6}$$

$$\cdot OH + Oxidative\ products \rightarrow CO_2 + H_2O \tag{7}$$

In this experiment, the maximum applied voltage setting is 10 V. An excessively high voltage will cause the current density to be too large to cause side reactions in the reaction system, thus hindering the electro-Fenton reaction, such as the hydrogen evolution reaction [26]. Furthermore, in terms of economic efficiency, at an excessively high voltage, the system would consume more energy and increase the cost of operation [27].
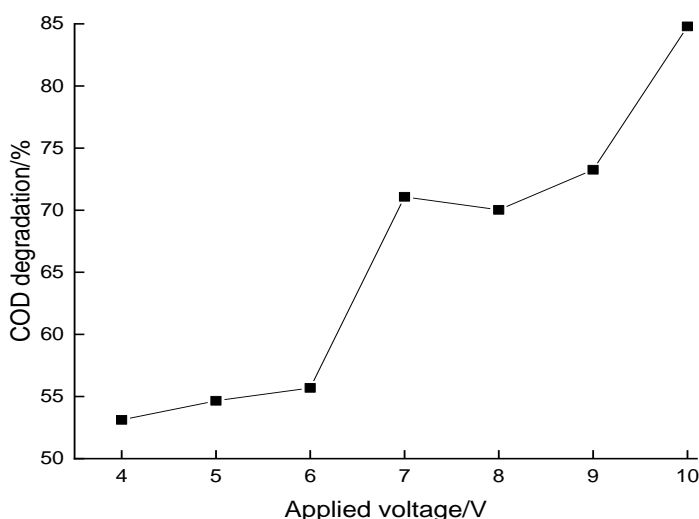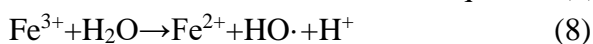

Figure 1. Effect of applied voltage on the removal efficiency of COD from the BTCW (initial pH=3; plate spacing=1 cm; reaction capacity=400 mL; reaction time=5 h).

3.1.2 Effect of initial pH

The initial pH of the reaction is one of the important parameters of the EF oxidation process. As shown in Figure 2, at a pH of 3, the COD treatment effect is at an optimal value of up to 85.1%. When the pH is less than 3, the COD removal rate starts at a low value and then increases as the pH increases. According to the Fenton reaction principle, when the H^+ concentration in the solution is too high, side effects will cause adverse effects, as described in the following two aspects [28,29]. On the one hand, Fe^{3+} cannot be efficiently reduced to Fe^{2+}. On the other hand, excessive consumption of $\cdot OH$ hinders the Fenton reaction, as shown in Equation (8) and Equation (9):

$$Fe^{3+} + H_2O \rightarrow Fe^{2+} + HO\cdot + H^+ \tag{8}$$

$$\cdot OH + H^+ + e^- \rightarrow H_2O \tag{9}$$

At a pH of approximately 3, the hydroxyl radical (•OH) is the most prevalent [20]. When the pH is more than 3, the COD removal rate shows varying degrees of decline with increasing pH value. As the pH increases, the stability of H_2O_2 deteriorates, leading to an accelerated rate of decomposition and accompanied by the formation of an iron hydroxyl complex [28].
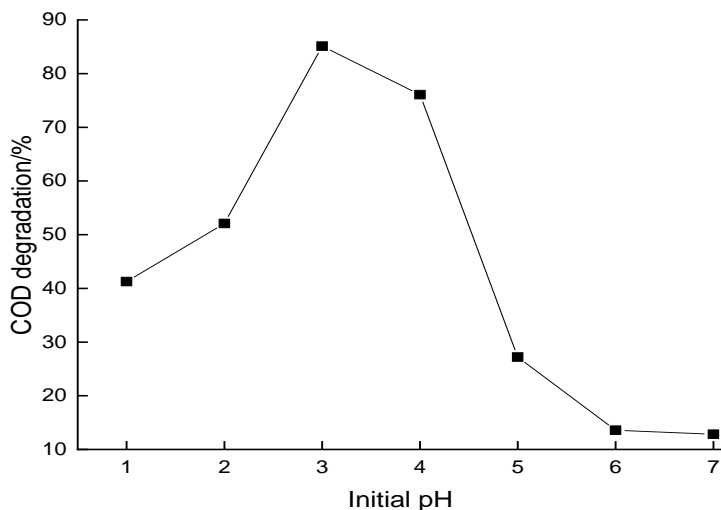

Figure 2. Effect of initial pH on the removal efficiency of COD from the BTCW (applied voltage=10 V; plate spacing=1 cm; reaction capacity=400 mL; reaction time=5 h).
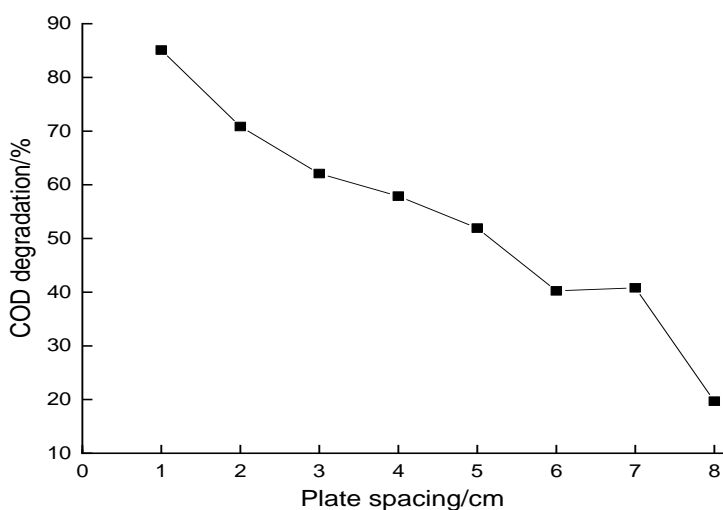
3.1.3 Effect of plate spacing

Figure 3. Effect of plate spacing on the removal efficiency of COD from the BTCW (applied voltage=10 V; initial pH=3; reaction capacity=400 mL; reaction time=5 h).

The plate spacing is also important in the EF oxidation process. As shown in Figure 3, the COD removal rate decreases as the plate spacing increases. The above analysis considers that the plate

spacing is related to the current density, which means that the current density decreases as the plate spacing increases [27]. The intensity of the current in the reaction determines the severity of the reaction. When the current density is low, the output of H_2O_2 and •OH decreases and affects the conversion rate of Fe^{2+}, thus reducing the processing effect of the system [28].

3.1.4 Effect of reaction time

As shown in Figure 4, the COD removal rate increases rapidly in the first three hours because the system provides a sufficient amount of oxidizing substances such as hydroxyl radicals; thus, the organic matter in the BTCW can be oxidized. The COD removal rate does not change significantly when the reaction time is extended from 3 to 5 h, demonstrating a basically stable value of approximately 83%. The reason is that the remaining organic bonds in the water sample are saturated, and thus, the structure is relatively stable. Hence, the reaction time is determined to be 3 h.
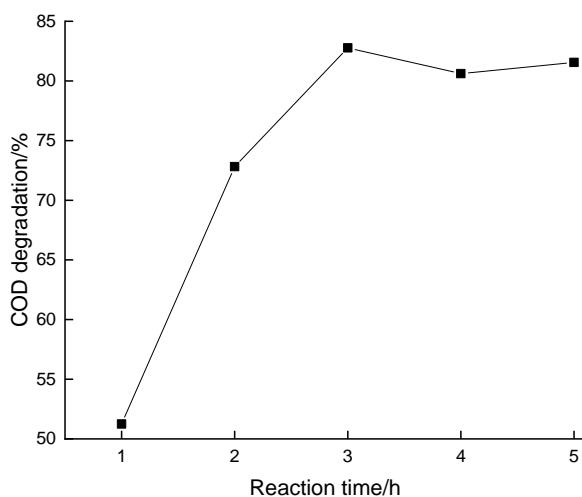

Figure 4. Effect of reaction time on the removal efficiency of COD from the BTCW (applied voltage=10 V; initial pH=3; plate spacing=1 cm; reaction capacity=400 mL).

3.2. Optimization

3.2.1 Model fitting

The factor design of the BBD experiment, the results of the experiment and the predictions about removing the COD are presented in Table 3. Five central point experiments (denoted as 0) are conducted to examine the repeatability of the experiment and obtain the standard deviation of the experimental response [30]. On this basis, the empirical relationship obtained between the response and the independent variable is represented by a second-order polynomial:

$Y=353.82–79.328X_1–10.243X_2+42.571X_3–1.667X_1X_2+5.023X_1X_3–2.4X_2X_3+4.125X_1{}^2+5.947X_2{}^2–13.198X_3{}^2$

Table 3. Box-Behknen experimental design and the results of COD removal

| | Real variables | | | COD removal efficiency (Y)/% | |
Run	X_1	X_2	X_3	Experimental (Y)/%	Predicted (Y)/%
1	8	1	3	86.67	87.84
2	10	1	3	100	104.49
3	8	3	3	78.34	73.85
4	10	3	3	85	83.83
5	8	2	2	60.09	62.94
6	10	2	2	66.67	66.2
7	8	2	4	60	60.47
8	10	2	4	86.67	83.82
9	9	1	2	76.67	72.65
10	9	3	2	58.49	60.13
11	9	1	4	86.67	85.03
12	9	3	4	58.89	62.91
13	9	2	3	79.1	77.43
14	9	2	3	70.07	77.43
15	9	2	3	78.84	77.43
16	9	2	3	80.04	77.43
17	9	2	3	79.1	77.43

3.2.2 ANOVA

The analysis of variance (ANOVA) was used to assess the significance and adequacy of the model. The correlation between the experimental and the predicted values was tested based on the value of R^2 and adjusted-R^2. The Fisher F test confirms whether the regression correlation coefficient is significant or not and finds significant variables in the model [25,31]. An analysis of the multivariate regression of the experimental data was used to obtain response surface plots of the regression model. Table 4 shows the response surface model fitting results. The relationship between the experimental data and predicted response is assessed by the multivariate correlation coefficient R^2 [32]. It can be seen from the table that the multivariate correlation coefficient R^2 is 0.9272, which indicates that the model can explain 92.72% of the total variability. The high R^2 coefficient validates the preferable adjustment of the experimental data by the polynomial model [33]. The correction correlation coefficient is applied to assess the suitability of the model. It can be seen from the table that the correction correlation coefficient adjusted-R^2 is 0.8336, which is not very different from the R^2 value; the above result indicates that the polynomial model has a good correction effect on the experimental data. An ideal model is that all experimental data should be placed above the fit [30]. The coefficient of variation (C.V. %) represents the dispersion of the experimental point relative to the predicted value of the model. the obtained C.V. % is 6.41%, and the C.V. % value for a good model should be less than 10%; thus the obtained result indicates that the model is reasonable and that the reliability and accuracy of the experimental data are high. A sufficient accuracy can measure the signal-to-noise ratio and compare the range of design point predictions with the average prediction error. When the ratio is

larger than 4, the model is ideal and exhibits sufficient discriminating power. In this work, the adequate precision value is 11.882, so the quadratic model can be adopted to guide the practice.

The magnitudes of the *F*-values and *p*-values represent the significance of the correlation coefficient. The *p*-value is below 0.0500, indicating that the model is statistically significant [25]. As shown in Table 4, the model *F*-value is 9.91, and the *p*-value is 0.0032. There is only a 0.32% chance that a "model *F*-value" this large can happen due to noise. Thus, it is implied that the model is significant, and the degree of fitting is good. If the model is statistically acceptable, the next step can be optimized. For a good model, a low *p*-value with a high *F*-value is desirable [32]. A lack of fit is one of the important factors used to estimate the reliability of a model. The *F*-value in the table is 1.89, indicating that the lack of fit is not significant. Due to noise, there is a 27.2% chance that "lack of fit *F*-value" this large could happen. The low lack of fit implies that the fitting effect in the response area is appropriate and can be used for data analysis [33].

In this model, X_1, X_2, X_2^2 and X_3^2 are significant parameters. According to the data analysis in Table 4, the applied voltage and plate spacing in the experiment are significant factors for the COD removal rate. However, the effect of pH is not significant, due to a *p*-value of 0.0636, but the square effect of pH is significant. When insignificant factors are excluded, the modified model fitting equation can be represented as follows:

$$Y=-66.937+6.655X_1-33.320X_2+81.671X_3+6.165X_2^2-12.98X_3^2$$

Although the simplified model highlights the impact of significant terms, it is also easy to ignore some details. Considering that the model has only three variables, the full model is still used for further research.

Table 4. ANOVA of the response surface quadratic model

Source	Sum of squares	DF	Mean square	F-value	p-value Prob>F	Remarks
Model	2112.90	9	234.77	9.91	0.0032	Significant
X_1	354.31	1	354.31	14.95	0.0062	Significant
X_2	600.14	1	600.14	25.33	0.0015	Significant
X_3	114.84	1	114.84	4.85	0.0636	
X_1X_2	11.12	1	11.12	0.47	0.5153	
X_1X_3	100.90	1	100.90	4.26	0.0779	
X_2X_3	23.04	1	23.04	0.97	0.3569	
X_1^2	71.64	1	71.64	3.02	0.1256	
X_2^2	148.94	1	148.94	6.29	0.0406	Significant
X_3^2	733.36	1	733.36	30.95	0.0008	Significant
Residual	165.85	7	23.69			
Lack of fit	97.30	3	32.43	1.89	0.2720	Not significant
Pure error	68.55	4	17.14			
Corrected total	2278.74	16				

$R^2=0.9272$; $R_{adj}^2=0.8336$; adequate precision=11.882; C.V. %=6.41%; DF=degrees of freedom.

P>*F*-value less than 0.0001 is highly significant; *P*>*F*-value less than 0.05 is significant; *P*>*F* - value greater than 0.05 is not significant.

3.2.3 Response surface and contour plotting

Figure 5(a) shows the response surface plot of the effect of the interaction between the applied voltage and initial pH on COD removal. It can be seen from the 3D plot that the COD removal rate decreases as the pH increases at a constant voltage. At a voltage of 10 V, the removal rate has a maximum value in a pH range of 2.5 to 3.

Figure 5(b) is a response surface plot of the interaction of the applied voltage and plate spacing on the COD removal rate. Compared with the plate spacing, the voltage has less effect on the COD treatment. From the variance analysis table, the F-value of the plate spacing is greater than that of the applied voltage. When the plate spacing is approximately 1 cm, the removal rate of the COD does not increase significantly with increasing voltage. Too high a voltage will make the current density too large, causing side reactions in the reaction system that hinder the EF reaction. Under the constraints of the experimental conditions, the highest value of the experimental voltage is set to 10 V [26].
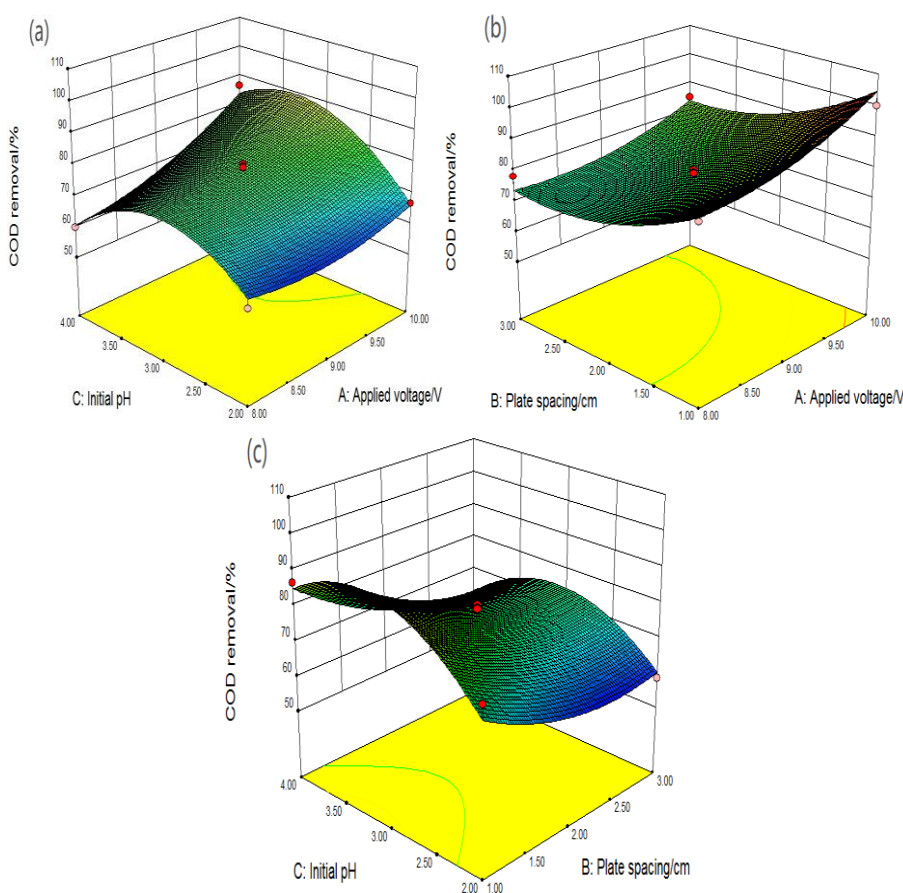

Figure 5. 3D plots showing the effect of applied voltage and initial pH (a), plate spacing and applied voltage (b), and initial pH and plate spacing (c).

Figure 5(c) is a response surface plot of the effect of plate spacing and initial pH interaction on the COD removal rate. It can be seen from the 3D diagram that when the distance between the plates is 1 cm, the treatment has a good treatment effect at an initial pH of 2-3. As the distance between the

plates increases, no matter how the initial pH changes, the result is lower than the plate spacing of 1 cm. The variation of the plate spacing is obviously greater than the change of the initial pH in the reaction, which also corresponds to the *p*-value of the plate spacing and the initial pH of the reaction in Table 4.

3.2.4 Optimization results

The main purpose of the experiment is to optimize the parameters to determine the optimal value of the three variables and obtain a maximum response value. According to the analysis of the established quadratic model and after applying a response optimization project in the design expert software, the optimal conditions are calculated to be 10 V, a plate spacing of 1 cm, and a pH of 3.42. Under optimal conditions, the model predicts a COD removal rate of 106.867%, while the experimental value of the COD removal rate is 99.2%. The error is 7.667%, explaining that this model can be successfully applied for optimizing the studied process.

In addition, chromaticity is an important pollution indicator for coking wastewater. The chromaticity of the BTCW before the reaction is approximately 50 times. After the HEF treatment, the color is equivalent to that of deionized water.

3.3. Stability of the Fe-AC-Ni composite electrode

To investigate the stability and the practical application potential of the electrode, five experiments were carried out continuously using the same Fe-AC-Ni composite electrode under the optimal conditions obtained above. After each experiment, the electrode was washed several times with deionized water and dried at 80 °C for 3 h before being used. The results show that the removal rates of COD are 89.9%, 94.9%, 97.5%, 100%, and 100%, indicating that the Fe-AC-Ni composite electrode is highly recyclable and has practical application potential. The phenomenon that the COD removal rate increases with the recycling times is unexpected and confusing. It is likely due to the microbubbles formed during the electrode preparation, which affects the conductivity of the electrode in the initial rounds but are gradually eliminated in the solution during later experiments.

3.4. Analytical characterization

3.4.1 Characterization of the Fe-AC-Ni composite cathode

Scanning electron microscopy (SEM) was used to observe the surface morphology of activated carbon and the iron-supported activated carbon in the composite electrodes after calcination at 300 °C in pure nitrogen. It can be clearly seen from Figure 6(a) that the surface of the activated carbon is smooth and that the pores are developed, which makes it a good support for the catalyst. There is no iron shown in the EDS analysis. Figure 6(b) shows that many small particles accumulate on the

surface. According to the EDS analysis, iron accounts for 0.8% by weight of the analysis area, which indicates that iron has successfully attached to the pores of the activated carbon.
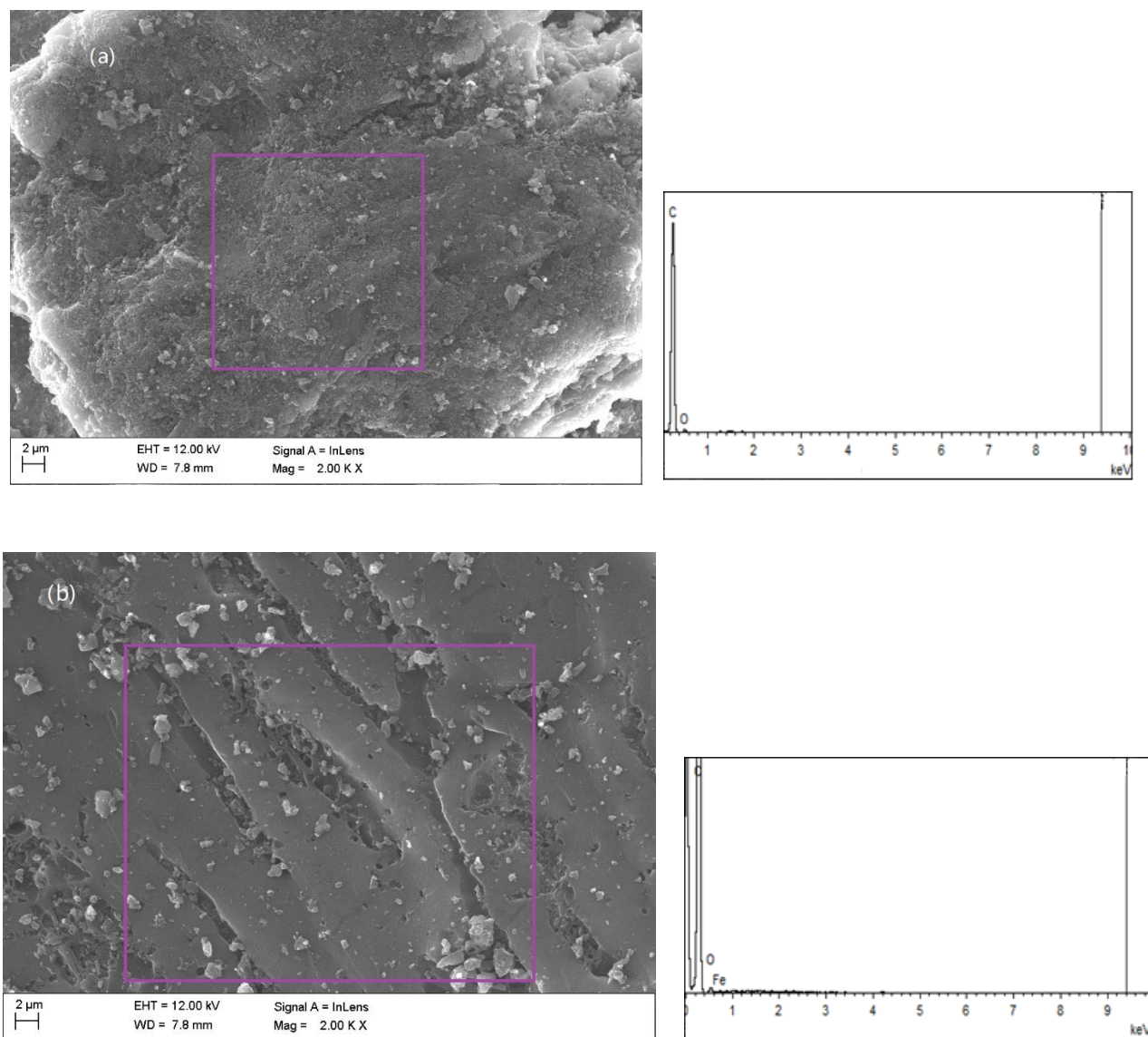

Figure 6. SEM and EDS analysis of the (a) activated carbon and (b) electrode material after loading.

3.4.2 Characterization of the BTCW treatment

According to the peak position and shape of the UV-Vis spectrum in Figure 7, the characteristic molecular structure contained in the solution can be obtained, and characteristics such as the aromaticity of the substance can be characterized. The BTCW shows strong absorption in a range of 220-250 nm, indicating that the component has a conjugated double bond. The only strong absorption peak is observed at 190 nm. An organic substance having a cyclic conjugated system in the ultraviolet region has an E absorption band and a B absorption band. The E absorption band is a

characteristic absorption band of an aromatic compound, and the B absorption band is a fine structure absorption band.
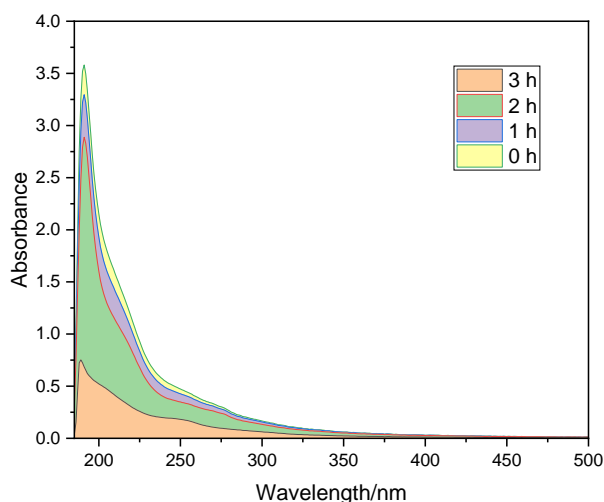

Figure 7. UV-Vis spectra of the BTCW treatment.

The E absorption band is produced by a benzene ring $\pi \rightarrow \pi^*$ transition and is a characteristic absorption band of an aromatic compound, which ranges from 185 to 210 nm. The B absorption band is also produced by a benzene ring $\pi \rightarrow \pi^*$ transition and ranges from 230 to 370 nm. Thus, the above observation is considered to be a cyclic aromatic compound. After reacting for 3 h through the HEF system, the absorption peak height of the sample at 190 nm is reduced to approximately one-seventh of the original height, thus demonstrating that the content of the aromatic cyclic compound is greatly reduced after the reaction.
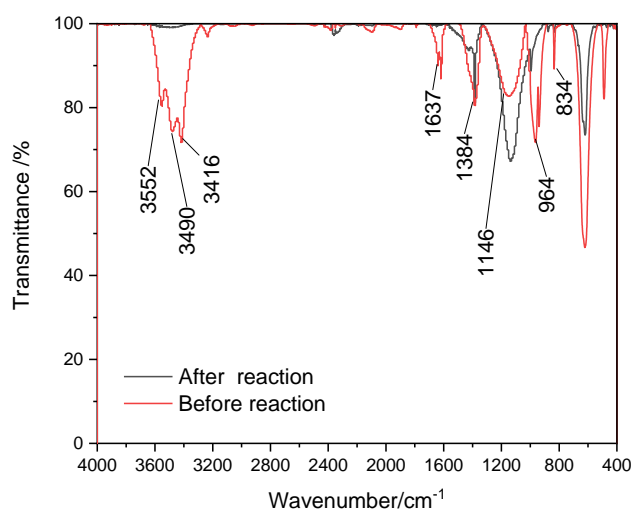

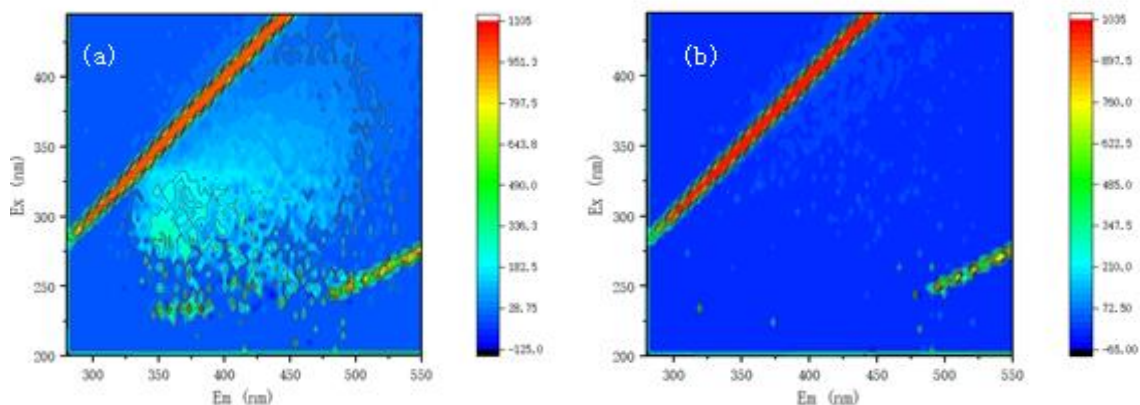**Figure 8**. FTIR spectra of the BTCW treatment.

Figure 9. 3D-EEM fluorescence spectra of the BTCW before (a) and after (b) treatment.

Figure 8 shows the FTIR spectra before and after the BTCW treatment. The spectra can be used to characterize the molecular groups and their structural information. Combined with 3D fluorescence spectroscopy, the types of organic matter contained in the sample can be determined[34]. The peaks at 3552 cm^{-1}, 3479 cm^{-1}, and 3416 cm^{-1} before the reaction indicate the presence of an O-H group. The functional group that corresponds to the characteristic peaks in a range of 3300 to 3600 cm^{-1} is a stretching vibration absorption peak of OH in COOH, alcohol, and phenol and can be considered as OH or an alcohol compound on COOH or a benzene ring. The skeleton vibration of aromatic C=C can be observed at 1637 cm^{-1}. The absorption peak at 1384 cm^{-1} indicates the presence of ethers, and the absorption peak at 1146 cm^{-1} indicates the presence of an alcohol compound. The absorption peak at 964 cm^{-1} is observed and is an absorption peak of a carboxylic acid or an ester, and the absorption peak at 834 cm^{-1} can be considered an olefin. Comparing the Fourier infrared spectrum before and after the treatment of the BTCW, the absorption peak of the BTCW at 3300-3750 cm^{-1} clearly disappears, which indicates that the content of hydroxyl groups has decreased after the reaction. From the spectrum in Figure 9, we can see that there are only two fluorescent peaks in the BTCW. One is a strong fluorescent peak located in the II region, which is judged to be an aromatic protein analog. The other position is a weak fluorescent peak located in the IV region, which is judged to be a microbial byproduct analog. After reacting for 3 h, the fluorescence peak in the IV region disappears completely, and only a small amount of fluorescent peaks exist in the II region[35]. Thus, only a small amount of carboxylic acids, alkanes, and halogenated hydrocarbons remain in the sample, and the final content is much lower than the initial content before the treatment. Basically, it can be considered that the organic matter is completely oxidized, and the effect is obvious, which confirms the treatment effect of the Fe-AC-Ni composite electrode when applied in the HEF system.
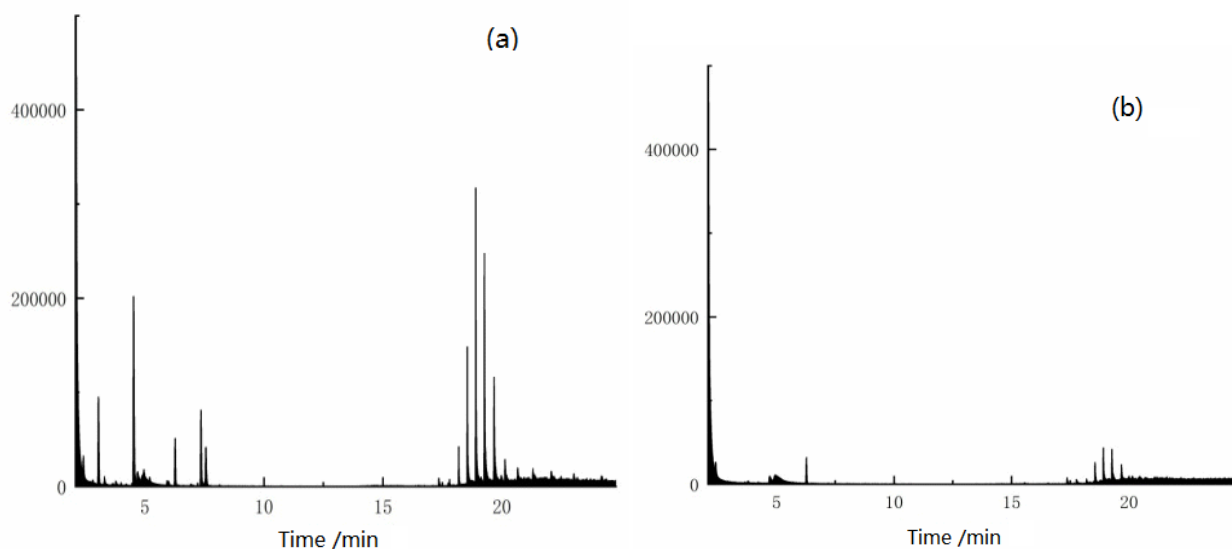
Figure 10. GC-MS of BTCW before (a) and after (b) treatment

GC-MS combines the strong separation ability of chromatographic techniques with the high discrimination ability of mass spectrometry to qualitatively identify mixtures. Figure 10 shows that there are 15 kinds of organic substances in the BTCW. Most of the organic matter in the BTCW is an alkane, a halogenated hydrocarbon, an ester and an amide compound. Among them, the largest proportion is made up of the alkane, and the content of the ester and amide is very small. After treatment, the amide and ester compounds are completely oxidized, and only a small amount of a long-chain alkane and a halogenated hydrocarbon compound remain. Thus, the Fe-AC-Ni composite electrode, when applied in the HEF system, can effectively remove esters and amide compounds from coking wastewater, which are difficult to dispose of via biochemical reactions.

4. CONCLUSIONS

In summary, we successfully prepared a Fe-AC-Ni composite electro-Fenton cathode, which when combined with a DSA anode, successfully processed the BTCW by HEF technology. The reusable potential of the cathode was revealed by repetitive experiments in continuous means. The operational parameters, including plate spacing, initial pH and applied voltage, were optimized using an RSM. The optimum process conditions were a plate spacing of 1 cm, an applied voltage of 10 V and an initial pH of 3.42, which resulted in a 99.2% COD removal. Spectral analysis showed that the novel electrode in the HEF process could effectively remove aromatic compounds, microbial byproduct analogs, olefins, alkynes and other compounds in the BTCW. Most of the remaining material after treatment was a long-chain alkane material.

References

1.   W. Zhang, C. Wei, X. Chai, J. He, Y. Cai, M. Ren, B. Yan, P. Peng, J. Fu, *Chemosphere*, 88 (2012) 174–182.
2.   W. Zhang, C. Wei, C. Feng, B. Yan, N. Li, P. Peng, J. Fu, *Sci. Total Environ.*, 432 (2012) 396–403.
3.   Y.M. Kim, D. Park, D.S. Lee, J.M. Park, *J. Hazard. Mater.*, 152 (2008) 915–921.
4.   M. Zheng, C. Xu, D. Zhong, Y. Han, Z. Zhang, H. Zhu, H. Han, *Chem. Eng. J.*, 364 (2019) 410–419.
5.   E. Rava, E. Chirwa, P. Allison, M. van Niekerk, M.P. Augustyn, *Water SA*, 41 (2015) 441–447.
6.   W. Xu, Y. Zhang, H. Cao, Y. Sheng, H. Li, Y. Li, H. Zhao, X. Gui, *Bioresour. Technol.*, 264 (2018) 106–115.
7.   E. Marañón, I. Vázquez, J. Rodríguez, L. Castrillón, Y. Fernández, H. López, *Bioresour. Technol.*, 99 (2008) 4192–4198.
8.   H. Zhu, Y. Han, C. Xu, H. Han, W. Ma, *Sci. Total Environ.*, 637–638 (2018) 1108–1126.
9.   X. Song, C. Wang, M. Liu, M. Zhang, *Water Sci. Technol.*, 77 (2018) 1891–1898.
10. N. Wang, T. Zheng, G. Zhang, P. Wang, *J. Environ. Chem. Eng.*, 4 (2016) 762–787.
11. P. Duan, X. Yang, G. Huang, J. Wei, Z. Sun, X. Hu, La $_2$ O $_3$ -CuO $_2$ /CNTs Electrode with Excellent Electrocatalytic Oxidation Ability for Ceftazidime Removal from Aqueous Solution, Elsevier B.V., (2019).
12. S. Garcia-Segura, J.A. Garrido, R.M. Rodríguez, P.L. Cabot, F. Centellas, C. Arias, E. Brillas, *Water Res.*, 46 (2012) 2067–2076.
13. S. Ahmed, M.G. Rasul, W.N. Martens, R. Brown, M.A. Hashib, *Desalination*, 261 (2010) 3–18.
14. V. de Oliveira Campos, *Int. J. Electrochem. Sci.*, 13 (2018) 7894–7906.
15. M. Panizza, M.A. Oturan, *Electrochim. Acta*, 56 (2011) 7084–7087.
16. S. Dharma, H.H. Masjuki, H.C. Ong, A.H. Sebayang, A.S. Silitonga, F. Kusumo, T.M.I. Mahlia, *Energy Convers. Manag.*, 115 (2016) 178–190.
17. W. Liu, Z. Ai, L. Zhang, *J. Hazard. Mater.*, 243 (2012) 257–264.
18. J. Fu, X. He, J. Zhu, W. Gu, X. Li, *Int. J. Electrochem. Sci.*, 13 (2018) 5872–5887.
19. L. Bounab, O. Iglesias, E. González-Romero, M. Pazos, M. Ángeles Sanromán, *RSC Adv.*, 5 (2015) 31049–31056.
20. E. Neyens, J. Baeyens, *J. Hazard. Mater.*, 98 (2003) 33–50.
21. W. Wu, Z.H. Huang, T.T. Lim, *Appl. Catal. A Gen.*, 480 (2014) 58–78.
22. R. Xie, M. Wu, G. Qu, P. Ning, Y. Cai, P. Lv, *J. Environ. Sci. (China)*, 66 (2018) 165–172.
23. X. Duan, P. Wu, K. Pi, H. Zhang, D. Liu, A.R. Gerson, *Int. J. Electrochem. Sci.*, 13 (2018) 5575–5588.
24. A. Kumar, B. Prasad, I.M. Mishra, *Chem. Eng. Technol.*, 30 (2007) 932–937.
25. Y. Zhang, Z. Tian, Q. Jing, Y. Chen, X. Huang, *Water Sci. Technol.*, 80 (2019) 308–316.
26. V.K. Sandhwar, B. Prasad, *Process Saf. Environ. Prot.*, 107 (2017) 269–280.
27. Q. Zhao, F. Wei, L. Zhang, Y. Yang, S. Lv, Y. Yao, *Water Sci. Technol.* (2019) 1–10.
28. B.P. Chaplin, *Environ. Sci. Process. Impacts*, 16 (2014) 1182–1203.
29. S. Bayu, *Environ. Prog. Sustain. Energy*, 30 (2012) 925–932.
30. Y. Sun, J.J. Pignatello, *Environ. Sci. Technol.*, 27 (1993) 304–310.
31. H. Zhang, C. Ye, X. Zhang, F. Yang, J. Yang, W. Zhou, *Water Sci. Technol.*, 66 (2012) 816–823.
32. G.B. Gholikandi, K. Kazemirad, *Water Sci. Technol.*, 77 (2018) 1765–1776.
33. M. Khosravi, S. Arabi, *Water Sci. Technol.*, 74 (2016) 343–352.
34. E. Brillas, I. Sire, M. a Oturan, I. Sirés, M. a Oturan, I. Sire, M. a Oturan, I. Sirés, M. a Oturan, *Chem. Rev.*, 109 (2009) 6570–6631.

35.   K.B. Wen Chen, Paul Westerhoff, Jerry A. Leenheer, *Environ. Sci. Technol.*, 37 (2003) 5701–5710.